BMC Medical Imaging

RESEARCH Open Access

Multiparametric radiomics signature for predicting molecular genotypes in adult-type diffuse gliomas utilizing ^{18}F-FET PET/MRI

Jie Bai[1,2], Bixiao Cui[1,2], Fengqi Li[1,2], Xin Han[1,2], Hongwei Yang[1,2] and Jie Lu[1,2*]

Abstract

Purpose This study aimed to investigate the utility of radiomic features derived from multiparametric O-(2-^{18} F-fluoroethyl)-L-tyrosine (^{18}F-FET) positron emission tomography (PET)/ magnetic resonance imaging (MRI) for the prediction of molecular genotypes in adult-type diffuse gliomas.

Methods This retrospective study analyzed 97 adult-type diffuse glioma patients, divided into 70% training and 30% testing cohorts. Each participant underwent hybrid PET/MRI scans, including FLAIR, 3D T1-CE, apparent diffusion coefficient (ADC), and ^{18}F-FET PET. After the multimodal images were spatially aligned, tumor segmentation was performed on the ^{18}F-FET PET and then applied to other MRI sequences. A total of 994 radiomic features were extracted from these specified modalities. The Naive Bayesian algorithm with five-fold validation was trained to develop prediction models for the IDH, TERT, and MGMT genotypes and to calculate the radiomics score (Rad-Score). The predictive performance of these models was evaluated via receiver operating characteristic (ROC) curves and decision curve analysis (DCA).

Results The combined model demonstrated superior performance compared to single-modality and MRI (FLAIR + T1-CE + ADC) models in predicting certain genotype statuses in the testing cohort (IDH AUC = 0.97, MGMT AUC = 0.86, TERT AUC = 0.90). The comparisons of the Rad-Score in multimodal models for identifying IDH, TERT, and MGMT showed significant differences (all $P < 0.001$). Performance of the radiomics signature surpassed that of clinical and conventional radiological factors. DCA indicated that all multimodal models provided good net clinical benefits.

Conclusions Multiparametric ^{18}F-FET PET/MRI comprehensively analyzes the structural, proliferative, and metabolic information of adult-type diffuse gliomas, enabling precise preoperative diagnosis of molecular genotypes. This has the potential to aid in the development of personalized clinical treatment plans.

Clinical trial number Not applicable.

Keywords Adult-type diffuse glioma, ^{18}F-FET, Radiomics, PET/MR, Genotype prediction

*Correspondence:
Jie Lu
imaginglu@hotmail.com
[1]Department of Radiology and Nuclear Medicine, Xuanwu Hospital, Capital Medical University, Beijing 100053, China
[2]Beijing Key Laboratory of Magnetic Resonance Imaging and Brain Informatics, Beijing 100053, China

Introduction

Adult-type diffuse gliomas, prevalent malignant neoplasms of the central nervous system, are known for their aggressive nature and poor prognosis. Glioblastoma patients generally have a median survival time between 12 and 15 months, yet a subset of patients may live for many years, which is predominantly influenced by the aggressiveness of tumors [1]. In recent years, significant advancements in tumor genetics have contributed to the discovery of many molecular biomarkers. The National Comprehensive Cancer Network guidelines highlight that molecular and genetic features are crucial for diagnosing and treating gliomas, which provide more information for diagnosis and prognosis, helping to select the optimal treatment strategies [2]. These biomarkers, characterized by their distinct diagnostic, prognostic, and therapeutic significance, have been instrumental in the molecular profiling of tumors and have offered directions for targeted treatment strategies [3].

Isocitrate dehydrogenase (IDH) plays a pivotal role in human metabolism, participating in crucial processes such as energy metabolism and the synthesis of vitamins, and amino acids [4, 5]. Notably, the presence of IDH mutations have been identified as an independent prognostic factor in gliomas associated with a favorable prognosis, which helps to improve survival outcomes and positive responses to therapy [6]. Telomerase reverse transcriptase (TERT), which encodes the catalytic subunit of the telomerase complex, is highly expressed because of mutations in the TERT promoter, thereby promoting the formation and malignant proliferation of gliomas [7]. Importantly, TERT promoter mutations, which are more common with increasing grade according to the World Health Organization (WHO) Classification of Tumors of the Central Nervous System (CNS), are associated with poorer overall survival in high-grade gliomas and act as an independent prognostic factor [8, 9]. O6-methylguanine-DNA methyltransferase (MGMT) is also a vital gene that encodes a protein essential for DNA repair mechanisms [10]. MGMT promoter methylation is associated with an enhanced response to temozolomide therapy and improved overall survival, especially in the elderly population with glioblastoma [11]. A study revealed that combining the IDH, TERT, and MGMT biomarkers improved the classification and prognostic stratification of gliomas across WHO grades 2 and 3 [12]. Consequently, the precise preoperative detection of these molecular biomarkers is crucial for accurate diagnosis, tailored treatment strategies, and prognostic assessment in glioma patients.

Owing to their remarkable target-to-background ratio (TBR), molecular imaging techniques utilizing positron emission tomography (PET) offer a detailed view of tumor amino acid metabolism, indicating potential in the delineation and guidance of treatment for gliomas [13–15]. Amino acid PET tracers, such as O-(2-^{18}F-fluoroethyl)-L-tyrosine (^{18}F-FET), which were recently endorsed by the Response Assessment in the Neuro-Oncology Working Group, are intended for incorporation into the clinical workflow for glioma management [16]. Conventional MRI sequences (e.g., FLAIR, ADC) provide structural information but lack sensitivity to metabolic heterogeneity, whereas ^{18}F-FET PET quantifies amino acid metabolism, reflecting tumor proliferation and angiogenesis [17]. Radiomics-based approaches are widely utilized in tumor staging, early diagnosis, differentiation, prognosis prediction, and treatment evaluation [18]. Therefore, radiomics, which is based on PET features, is becoming increasingly important in the initial diagnosis of gliomas. However, only a few studies have utilized the recommended amino acid tracers for their assessment [19]. This noninvasive technique allows for the assessment of metabolism across the entire tumor, in contrast to histopathological examinations that focus on specific tumor regions. Nevertheless, single-modality models (e.g., PET-Rad Model) exhibit limited predictive performance [20]. Multiparametric PET/MR radiomics overcomes these limitations by integrating metabolic and structural heterogeneity. Kaiser et al. [21] demonstrated that combining PET texture features with MRI parameters significantly improved IDH mutation prediction (AUC = 0.94).

Given that prior studies have primarily focused on using MRI-based radiomics methods to predict individual genetic alterations, the effectiveness of radiomics methods in detecting multiple glioma biomarkers within multiparametric ^{18}F-FET PET/MR data remains to be fully validated. In this study, we aimed to further explore the potential of radiomics features derived from ^{18}F-FET PET and multiparametric MRI (FLAIR, T1-CE, and ADC) in predicting three key molecular biomarkers (IDH, TERT, and MGMT) for adult-type diffuse gliomas.

Materials and methods

Study participants

In accordance with the Declaration of Helsinki, this retrospective study was approved by the Ethics Committee and Institutional Review Board of Xuanwu Hospital, Capital Medical University (No. 2023-044). Written informed consent was obtained from patients prior to PET/MR scans.

Patients who were diagnosed with adult-type diffuse gliomas at our hospital from March 2019 to June 2024 were enrolled in the cohort (Fig. 1). The inclusion criteria were as follows: (1) patients with histologically confirmed adult-type diffuse gliomas who had complete molecular analysis (including IDH, TERT, and MGMT) prior to surgical resection or biopsy; and (2) patients with hybrid

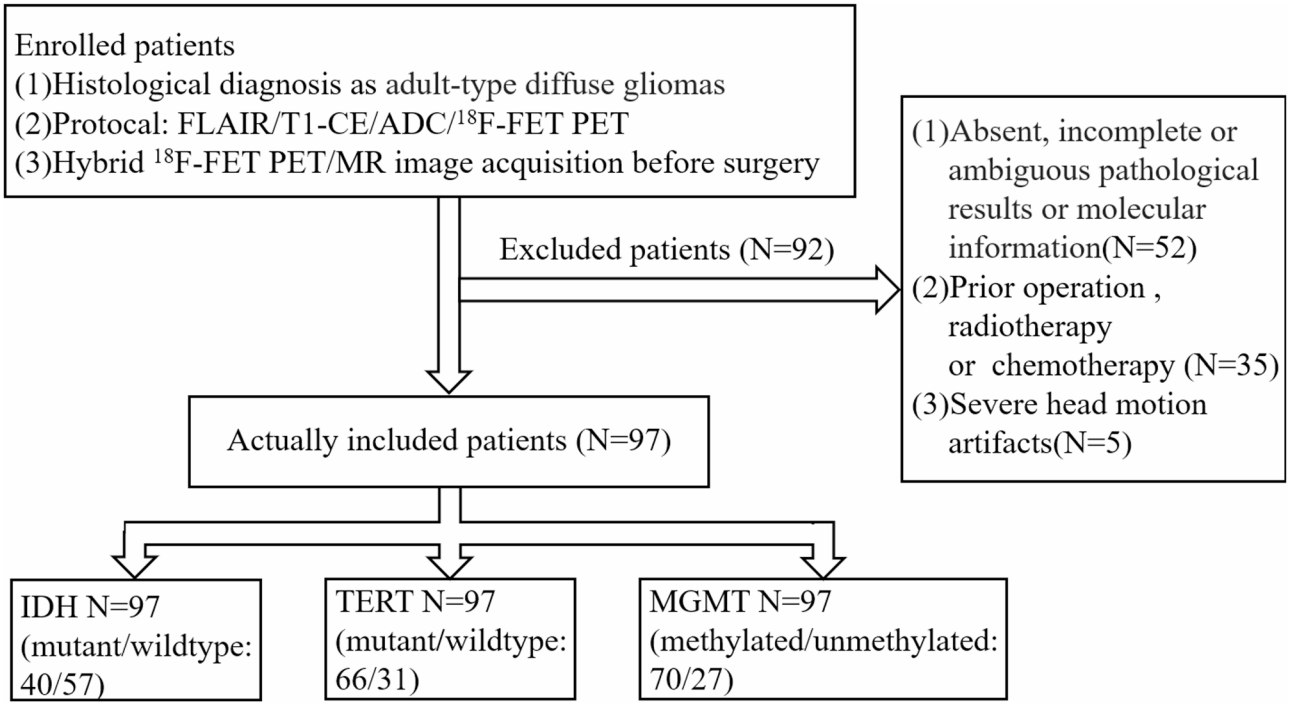

Fig. 1 Flowchart of the study population

^{18}F-FET PET/MR image acquisition before surgery. The exclusion criteria were as follows: (1) absent, incomplete or ambiguous pathological results or molecular diagnostic information (IDH, TERT, and MGMT); (2) prior operation, radiotherapy or chemotherapy before PET/MR scan; and (3) severe head motion artifacts. Ultimately, the trial included a total of 97 participants, who were randomly split into training and testing cohorts at a ratio of 7:3.

Hybrid ^{18}F-FET PET/MR image

Simultaneous ^{18}F-FET PET/MR images were obtained on a 3-T hybrid PET/MR system (GE Signa, GE Healthcare, USA) via a 19-channel head and neck union coil. Each participant received an intravenous injection of approximately 200 MBq of ^{18}F-FET while remaining fasted for at least 4 h before the PET/MR scan. The MRI protocols included axial fluid-attenuated inversion recovery (FLAIR), axial diffusion-weighted imaging (DWI), and 3D contrast-enhanced T1-weighted magnetic resonance imaging (T1-CE). The specific MRI parameters included FLAIR (repetition time (TR)/ echo time (TE) = 6200/140 ms, slice = 22, voxel size = 1.00 × 1.00 × 5.00 mm^3), DWI (TR/TE = 5000/Minimum ms, with b values of 1000 s/mm^2, slice = 44, voxel size = 1.30 × 1.30 × 5.00 mm^3) and 3D T1-CE (TR/TE = 2100/Minimum ms, slice = 188, voxel size = 1.00 × 1.00 × 1.00 mm^3). The apparent diffusion coefficient (ADC) map was generated from the DWI data via the AW 4.7 workstation (GE Healthcare). Static PET brain data were acquired 20 min postinjection, with a total acquisition time of 20–40 min. The PET data were reconstructed via a Dixon scan for MRI-based attenuation correction, yielding a 256 × 256 matrix with a 35 cm field of view and voxel dimensions of 1.36 × 1.36 × 2.78 mm^3. This reconstruction integrates the time-of-flight, point spread function and ordered subset expectation maximization algorithms and employs 6 iterations and 16 subsets.

Histological evaluation and molecular analysis

Tissue samples were collected from patients during resection and fixed with paraffin. The sample sections were subsequently used for neuropathological diagnosis and molecular assessment, with the classification and grading of the included adult-type diffuse gliomas reconfirmed according to the WHO 2021 classification of CNS tumors by two experienced pathologists. The detection of the IDH and TERT promoter mutation status, as well as the MGMT promoter methylation status, began with PCR amplification. Next, Sanger sequencing was used to determine the mutation status of IDH and TERT, while real-time quantitative PCR was employed for quantitative analysis of the methylation levels in the promoter region of the MGMT gene.

Data preprocessing and feature extraction

The workflow steps used for processing are illustrated in Fig. 2. Preprocessing of PET/MRI data was performed via the MATLAB R2021a and SPM12 software environments. To rectify the uneven intensity distribution within

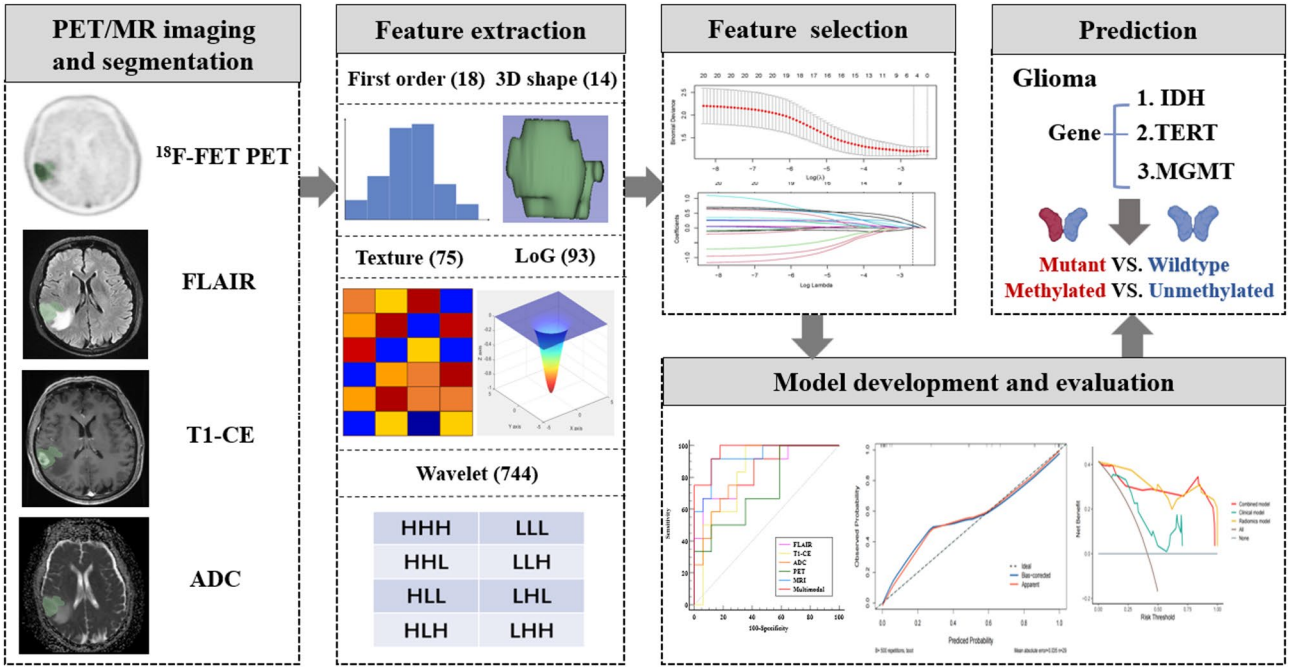

Fig. 2 Workflow steps in processing

multiparametric MR images, N4 bias field correction was applied. Afterward, FLAIR, ADC, and ^{18}F-FET PET images were resampled to a voxel size of 1.00 × 1.00 × 1.00 mm^3, aligning them with the 3D T1-CE image via standard rigid-body settings for robust coregistration.

In the process of tumor segmentation, 3D Slicer software (version 5.4.0, https://www.slicer.org) was used to delineate the volume of interest (VOI) in ^{18}F-FET PET images by applying a TBR threshold greater than 1.6 within the tumor lesion area [22]. The mean background activity of ^{18}F-FET PET was assessed via a large, crescent-shaped VOI placed in the unaffected contralateral hemisphere, encompassing both white and gray matter, as published earlier [21]. Several PET quantitative metrics, including the maximal standardized uptake value (SUV_{max}) and mean SUV (SUV_{mean}), as well as the maximal TBR (TBR_{max}) and mean TBR (TBR_{mean}), were calculated by the basis of the VOI from PET imaging as previously described [23]. Similarly, the values of minimum ADC (ADC_{min}) and mean ADC (ADC_{mean}) were derived from VOI analysis of the ADC image. Two experienced radiologists, blinded to the final diagnoses and molecular biomarker status, reviewed the VOI segmentation and reached a consensus. Disagreements were resolved by a third senior physician.

A total of 994 features were extracted from each modality, including first-order (18), 3D shape (14), texture (75), Laplacian of Gaussian (LoG) (93) and wavelet transformed features (744) via Python software (version 3.9, https://www.python.org). A set of 994 imaging fea tures was extracted, including textural and non-textural features. The extraction of texture features involves various methods, such as the gray level co-occurrence matrix (GLCM), gray level run length matrix (GLRLM), gray level size zone matrix (GLSZM), and neighboring gray tone difference matrix (NGTDM).

Feature selection and model construction

To enhance the interpretability and generalization capabilities of the prediction models, two feature selection methods were utilized: minimum redundancy maximum relevance (mRMR) and least absolute shrinkage and selection operator (LASSO). The mRMR algorithm was employed to maximize the correlation between features and the target variable while minimizing redundancy among features, thereby enhancing model interpretability and reducing the risk of overfitting. Subsequently, LASSO, a feature selection method based on L1 regularization, could automatically identify key features in high-dimensional data and mitigates multicollinearity. By combining both methods, we balanced feature independence and model generalizability, ensuring robustness in our radiomics pipeline. Naive Bayesian algorithms were used to establish three five-fold validation machine learning models to calculate radiomics score (Rad-score), which were useful for predicting the IDH, TERT, and MGMT genotypes in all patients. Single-modality models based on radiomics features extracted from multiparametric PET/MR images were constructed for FLAIR, ADC, T1-CE, and ^{18}F-FET PET. The MRI model integrated features from FLAIR, T1-CE, and ADC, whereas a multimodal model combined all features from PET/

MRI. Each model was applied individually to predict biomarker status. In the clinical model, clinical features included both clinical and MR imaging characteristics, along with ADC and PET. More detailed information can be found in Table S1. Ultimately, optimal clinical features were identified through univariate analysis and refined via stepwise multivariate logistic regression to construct a clinical model. The combined model incorporated both radiomics features and selected clinical characteristics.

Statistical analysis

R software (version 3.6.1, https://www.r-project.org) was used for the statistical analysis. Receiver operating characteristic (ROC) curves and the area under the curve (AUC) were obtained to evaluate the performance of all the models within each molecular group, along with 95% confidence interval (CI), sensitivity (SEN), specificity (SPE) and accuracy (ACC). Decision curve analysis (DCA) was conducted to evaluate the clinical utility of each model in the testing cohort by assessing the net benefit across a range of threshold probabilities.

Differences in clinical characteristics and imaging features among each genotype were compared using IBM SPSS Statistics (version 27). Descriptive statistics for continuous data are presented as mean and standard deviation, while categorical data are reported in terms of frequencies. For variables with a normal distribution (e.g., age), an independent samples t-test was applied. Then, the Mann-Whitney U test was used to assess differences in continuous data that exhibited non-normal distributions. Significance of categorical variables was determined using chi-square or Fisher's exact tests. $P < 0.05$ was considered to indicate statistical significance.

Table 1 Demographic characteristics of patients in training and test cohort

Characteristics	Training cohort ($N = 68$)	Testing cohort ($N = 29$)	*P*-value
Age	50.97 ± 14.63	51.72 ± 12.54	0.809[a]
Gender (M/F)	40/28	13/16	0.739[b]
WHO Grade			0.908[b]
2	15	7	
3	10	5	
4	43	17	
IDH			0.985[b]
Mutant	28	12	
Wild-type	40	17	
TERT			0.546[b]
Mutant	45	21	
Wild-type	23	8	
MGMT			0.340[b]
Methylated	51	19	
Unmethylated	17	10	

Note: Data are presented as means ± standard deviation. IDH, Isocitrate dehydrogenase; TERT, Telomerase reverse transcriptase; MGMT, O6-methylguanine-DNA methyltransferase

[a]Independent samples t-test. [b]Chi-square test

Results

Patient demographic characteristics

The demographic and clinical characteristics of the enrolled participants in the training cohort ($N = 68$) and testing cohort ($N = 29$) are shown in Table 1. The cohort comprised 57 males and 42 females with a mean age of 51.20 ± 13.98 years. No significant differences in patient characteristics were observed between the training and testing groups in terms of age, sex, grade or molecular biomarker status, which justified their applicability.

Radiomics feature selection and Rad-Score

Following Naive Bayesian analysis, multimodal predictive models were developed for each molecular biomarker. These models incorporated 13 radiomics features for IDH, 12 for TERT, and 13 for MGMT, including first-order statistics, texture features, and wavelet features. The results are listed in Table S2. The IDH-mutant group had a significantly higher Rad-score than the IDH wild-type group in multimodal models ($P < 0.001$). A similar pattern was observed between the TERT promoter-mutant and TERT promoter wild-type groups ($P < 0.001$). Additionally, patients with MGMT promoter methylation had a higher Rad-score than those with MGMT promoter unmethylation in multimodal models ($P < 0.001$). The comparisons of the Rad-Score in multimodal models for each biomarker are shown in Fig. 3. Representative cases are shown in Fig. 4.

Assessment of prediction model

The predictive models were evaluated for their performance in determining the status of IDH, TERT, and MGMT via PET/MR radiomics, which included single modality (FLAIR, T1-CE, ADC, and ^{18}F-FET PET), MRI (FLAIR + T1-CE + ADC), and multimodal models (FLAIR + T1-CE + ADC + ^{18}F-FET PET). The results are shown in Tables 2 and 3, and Fig. 5. We found that the multimodal models performed better in identifying the molecular genotypes than both the single modality and the MRI models. In the prediction of the IDH genotype, the multimodal model demonstrated superior performance (AUC = 0.97, ACC = 90.0%) in the testing cohort, which was higher than that of the single modality (FLAIR, AUC = 0.84, ACC = 82.8%; T1-CE, AUC = 0.83, ACC = 79.3%; ADC, AUC = 0.82, ACC = 75.9%; ^{18}F-FET PET, AUC = 0.73, ACC = 65.5%), and the MRI model (AUC = 0.93, ACC = 89.7%). With respect to the TERT genotype, the multimodal model showed better predictive performance (AUC = 0.86, ACC = 75.9%) than the single modality (FLAIR, AUC = 0.76, ACC = 72.4%; T1-CE, AUC = 0.73, ACC = 79.3%; ADC, AUC = 0.73,

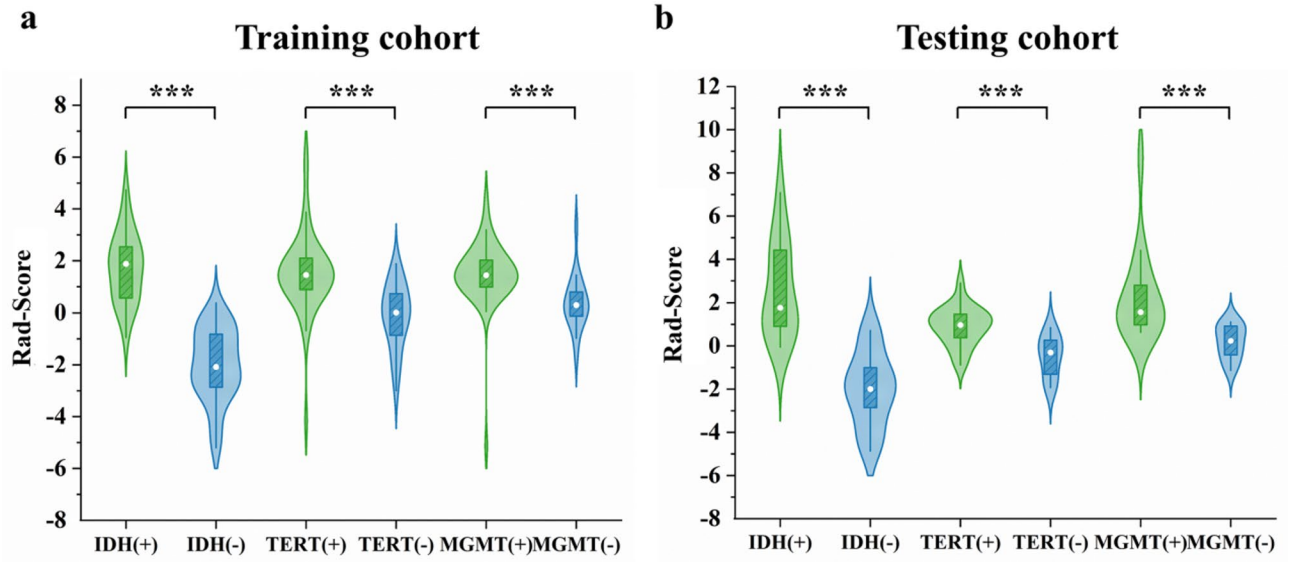

Fig. 3 Rad-scores of participants in multimodal models for each biomarker. Rad-scores of multimodal models for distinct statuses of IDH, TERT and MGMT in the training (**a**) and testing (**b**) cohorts (all $P < 0.001$). ***$P < 0.001$

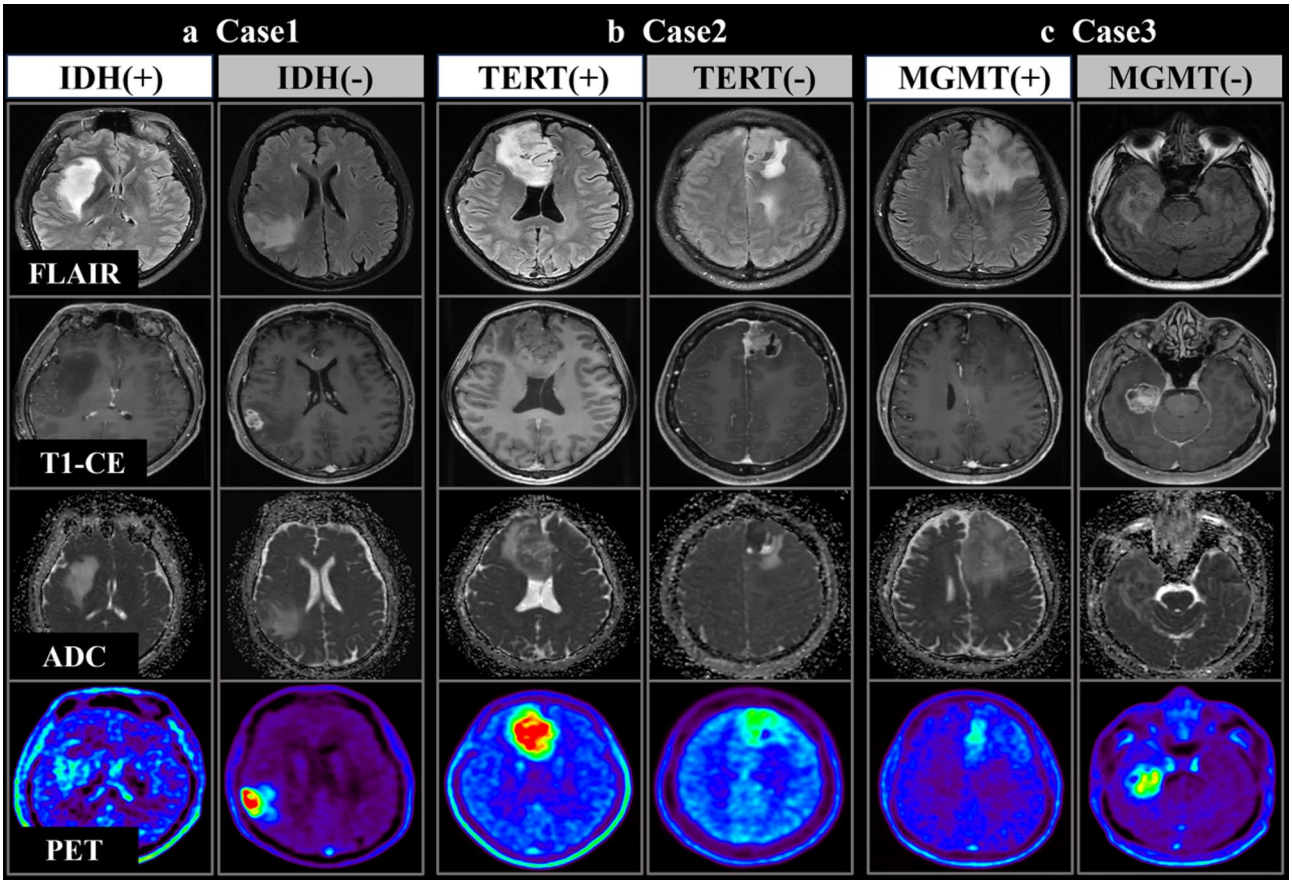

Fig. 4 Typical cases of the classification results. After segmentation and feature extraction, decision values were computed according to our ^{18}F-FET PET/MR radiomics predictive models. Case 1: IDH-mutant astrocytoma (Rad-score = 2.166) versus IDH wild-type glioblastoma (Rad-score = -1.287). Case 2: TERT-mutant oligodendroglioma (Rad-score = 1.857) versus TERT wild-type glioblastoma (Rad-score = -0.949). Case 3: MGMT-methylated astrocytoma (Rad-score = 1.665) versus MGMT-unmethylated glioblastoma (Rad-score = -0.584)

Table 2 Predictive performance of unimodal models for each biomarker

	IDH				TERT				MGMT			
	FLAIR	T1-CE	ADC	^{18}F-FET	FLAIR	T1-CE	ADC	^{18}F-FET	FLAIR	T1-CE	ADC	^{18}F-FET
Training												
AUC	0.87	0.90	0.87	0.78	0.78	0.72	0.72	0.77	0.79	0.78	0.78	0.80
95%CI												
Lower	0.78	0.82	0.79	0.66	0.66	0.59	0.59	0.66	0.66	0.67	0.66	0.67
Upper	0.96	0.97	0.96	0.89	0.90	0.85	0.85	0.88	0.92	0.9	0.89	0.93
ACC(%)	79.4	88.2	79.4	77.9	70.6	70.6	72.1	70.6	69.1	76.5	63.2	70.6
SEN(%)	89.3	78.6	92.9	67.9	64.4	75.6	82.2	62.2	64.7	76.5	51.0	64.7
SPE(%)	72.5	95.0	70.0	85.0	82.6	60.9	52.2	87.0	82.4	76.5	100.0	88.2
Testing												
AUC	0.84	0.83	0.82	0.73	0.76	0.73	0.73	0.76	0.79	0.75	0.77	0.80
95%CI												
Lower	0.69	0.67	0.66	0.53	0.57	0.49	0.53	0.55	0.60	0.56	0.56	0.63
Upper	0.99	0.98	0.97	0.92	0.96	0.96	0.93	0.97	0.98	0.94	0.97	0.96
ACC(%)	82.8	79.3	75.9	65.5	72.4	79.3	62.1	79.3	79.3	72.4	75.9	72.4
SEN(%)	66.7	100.0	75.0	100.0	66.7	85.7	52.4	85.7	78.9	63.2	73.7	63.2
SPE(%)	94.1	64.7	76.5	41.2	87.5	62.5	87.5	62.5	80.0	90.0	80.0	90.0

Note: AUC, the area under the receiver operating characteristic curve; CI, confidence interval; ACC, accuracy; SEN, sensitivity; SPE, specificity

ACC = 62.1%; ^{18}F-FET PET, AUC = 0.76, ACC = 79.3%) and the MRI model (AUC = 0.81, ACC = 82.8%) in the testing cohort. In the prediction of the MGMT genotype, the multimodal model yielded AUC = 0.90 and ACC = 79.3% in the testing cohort, which is greater than those of the single modality (FLAIR, AUC = 0.79, ACC = 79.3%; T1-CE, AUC = 0.75, ACC = 72.4%; ADC, AUC = 0.77, ACC = 75.9%; ^{18}F-FET PET, AUC = 0.80, ACC = 72.4%) and MRI models (AUC = 0.85, ACC = 79.3%).

Assessment of clinical model

A comparison of the clinical and MRI imaging features of the genotype status of each molecular biomarker is summarized in Table S1. After univariate analysis and multivariate logistic regression were performed, the differences in the following characteristics were found to be significant and are detailed in Table S3. The results revealed that age (OR = 0.93, 95% CI, 0.89–0.97; $P < 0.001$) and the ADC_{min} (OR = 1.01, 95% CI, 1.00-1.01; $P < 0.001$) were significantly associated with the IDH mutation status. The clinical feature of TBR_{max} (OR = 3.20, 95% CI, 1.73–5.93; $P = 0.001$) was closely related to TERT promoter mutation. MGMT promoter methylation was more likely to involve the frontal lobe (OR = 2.95, 95% CI: 1.06–8.19; $P = 0.038$) than the unmethylated status was. Clinical and combined models for each biomarker were subsequently established, as shown in Table S4. The AUC values for the clinical and combined models in identifying molecular genotypes across the training/testing cohorts were as follows: IDH, AUC (0.81/0.96); TERT, AUC (0.80/0.83); and MGMT, AUC (0.64/0.87). Nevertheless, incorporating clinical variables into the multimodal radiomics features did not lead to a significant improvement in the predictive performance for molecular genotypes within the combined model that incorporated both radiomics features and selected clinical characteristics.

The decision curve analysis revealed that multimodal model had a higher threshold probability for benefiting across the range of 0–1 than the clinical model for each biomarker, yet it was nearly equivalent to the combined model, as depicted in Fig. 6.

Discussion

In this study, we explored the potential of a multiparametric radiomics signature based on ^{18}F-FET PET/MRI to predict molecular biomarker genotypes in adult-type diffuse gliomas. Our multimodal prediction models, which integrate structural, proliferative, and metabolic information from PET/MRI radiomics, employed Naive Bayesian algorithm to significantly improve the diagnostic performance for multiple genotypes (IDH, TERT and MGMT). In the training cohort, the accuracy values for predicting the IDH, TERT, and MGMT genotypes

Table 3 Performance of fusion models for each biomarker status

	IDH		TERT		MGMT	
	Multimodal	**MRI**	**Multimodal**	**MRI**	**Multimodal**	**MRI**
Training						
AUC	0.98	0.95	0.84	0.81	0.91	0.86
95%CI	0.96 - 1.00	0.91 - 1.00	0.75 - 0.94	0.68 - 0.93	0.84 - 0.99	0.77 - 0.95
ACC(%)	95.6	91.2	82.4	77.9	86.8	77.9
SEN(%)	92.9	89.3	84.4	73.3	86.3	74.5
SPE(%)	97.5	92.5	78.3	87.0	88.2	88.2
Testing						
AUC	0.97	0.93	0.86	0.81	0.90	0.85
95%CI	0.91-1.00	0.83-1.00	0.71-1.00	0.57-1.00	0.79-1.00	0.71-1.00
ACC(%)	90.0	89.7	75.9	82.8	79.3	79.3
SEN(%)	100.0	91.7	71.4	81.0	68.4	78.9
SPE(%)	82.4	88.2	87.5	87.5	100.0	80.0

Note: AUC, the area under the receiver operating characteristic curve; CI, confidence interval; ACC, accuracy; SEN, sensitivity; SPE, specificity

reached 95.6%, 82.4%, and 86.8%, respectively. Comparatively, the testing cohort demonstrated accuracy values of 90.0%, 75.9%, and 79.3% for predicting these genotypes.

The updated WHO 2021 classification of CNS tumors highlights the importance of molecular biomarkers in the diagnosis and management of gliomas [24]. The incorporation of specific molecular groups, such as IDH and TERT status, into tumor grading has significantly improved the prognostic evaluation of gliomas [25]. MGMT promoter methylation serves as a robust prognostic indicator in glioma patients, especially with respect to the chemosensitivity of IDH wild-type glioblastomas [26]. Amino acid PET tracers, like ^{18}F-FET PET, have shown value in evaluating intratumoral heterogeneity, as their uptake correlates with cellular proliferation and microvascular density [17]. ^{18}F-FET PET has proven effective in revealing tumor molecular characteristics, with significant potential for clinical applications in gliomas, including grading, subtyping, and treatment evaluation [17, 27, 28, 29, 30].

Nevertheless, conventional FET imaging features face certain limitations in precise diagnostics. Song et al. [31] reported that TBR from ^{18}F-FET PET and cerebral blood flow from arterial spin labeling were ineffective in determining the MGMT status. Similarly, a retrospective study involving one hundred IDH-wildtype glioblastoma patients revealed that neither static nor dynamic ^{18}F-FET PET parameters were successful in predicting TERT promoter mutations [32]. In contrast, our study demonstrated that the single-modality model based on ^{18}F-FET PET radiomics analysis exhibited good predictive performance for identifying the TERT and MGMT genotypes in the testing cohort, with AUC of 0.76 and 0.80, respectively. Feature selection using mRMR and LASSO prioritized first-order statistics, texture, and wavelet features over conventional PET metrics (e.g., TBR_{max}). This indicates that metabolic heterogeneity, rather than SUV values, may better reflect the underlying biological characteristics of different TERT and MGMT status. This finding aligns with prior studies, where first-order statistics and textural features of PET outperformed traditional parameters [33, 34].

To date, the majority of research has focused only on MRI-based radiomics to predict molecular biomarkers. For instance, a study based on multiparametric MRI radiomics features reported an AUC of 0.795 in predicting IDH mutation status, achieving moderate performance [35]. However, limitations persist, such as the limited accuracy of TERT prediction (AUC: 0.669, accuracy: 65.5%) [36] and incomplete characterization of tumor heterogeneity. Our study integrated ^{18}F-FET PET into radiomics models, resulting in superior performance in the testing cohorts (IDH AUC = 0.97, TERT AUC = 0.86, and MGMT AUC = 0.90) compared with single modality and MRI models. These findings confirm that ^{18}F-FET PET provides valuable insights into tumor amino acid metabolism, effectively supplementing MRI data.

Additionally, the multimodal radiomics features we proposed achieved superior prediction performance when compared with clinical and conventional radiological factors. Firstly, our fusion signature from multimodal information, which included more comprehensive information that reflects subtle textural differences in the microenvironments and obtained important imaging characteristics associated with multiple glioma genotypes, outperformed those derived from individual sequences. Secondly, most of the effective features extracted in our study were textural and wavelet features, which enabled multi-scale analysis of tumor texture and structure. Thus, these images more effectively captured key tumor heterogeneity and spatial distribution. Moreover, research verified by histopathology has shown that areas of high metabolic activity in gliomas, as identified

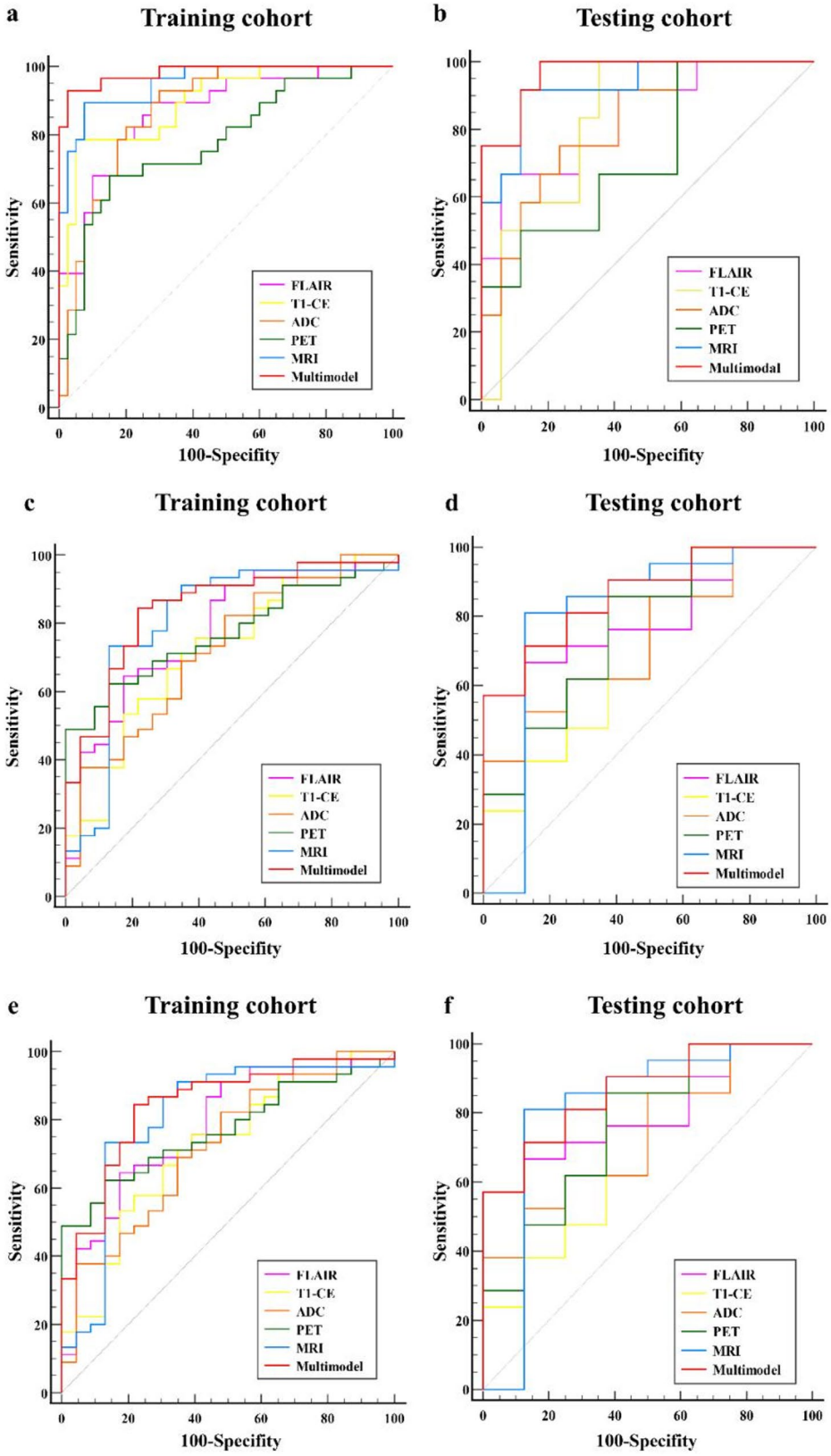

Fig. 5 The ROC of the machine learning models. **a** and **b**, ROC curve for the prediction of IDH (mutant or wild type); **c** and **d**, ROC curve for the prediction of TERT (mutant or wild type); **e** and **f**, ROC curve for the prediction of MGMT (methylated or unmethylated); MRI, MRI model (FLAIR + T1-CE + ADC); multimodal model, (FLAIR + T1-CE + ADC + ^{18}F-FET PET); ROC curve, receiver operating characteristic curve

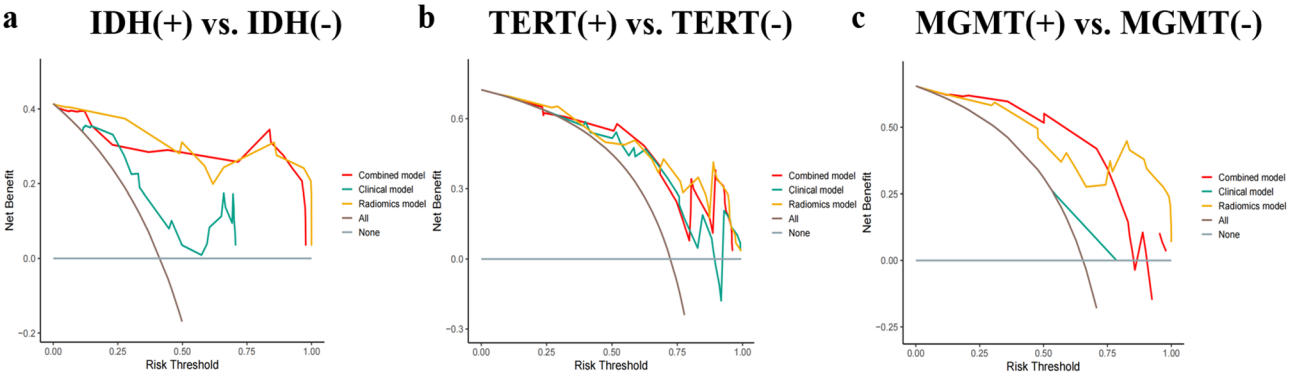

Fig. 6 The results of decision curve analysis. The DCA of the radiomics models, clinical models and combined model in the testing cohort for the prediction of the IDH (**a**), TERT (**b**), and MGMT (**c**) genotypes. Radiomics model (multimodal model, yellow curve), clinical model (green curve) and combined model (red curve)

by ^{18}F-FET PET, frequently extend beyond the tumor volumes observed on CE-MRI [13]. Therefore, we adopted this method from previous studies [14, 34], which defined the entire tumor volume on ^{18}F-FET PET as the VOI and applied it synchronously to MRI sequences. The radiomics approach applied to multiparametric PET/MRI data may better reflect overall lesion characteristics, leading to improved diagnostic efficiency.

Furthermore, we also explored whether a combined model incorporating clinical variables, radiological variables, and fusion radiomics signature would outperform the signature alone. In our study, age and ADC_{min} were significant predictors of the IDH genotype, frontal lobe involvement was a key predictor of the MGMT genotype, and TBR_{max} was a crucial predictor of the TERT genotype in glioma. However, incorporating these variables into multimodal radiomics did not yield any improvement in performance. This lack of improvement may be due to the subjective nature of some variables, which are influenced by radiologists' judgment, or because these variables only roughly represent certain tumor characteristics. Additionally, the inherent heterogeneity of tumors means that these parameters cannot fully capture phenotype information. Therefore, adding these factors to radiomics features does not enhance predictive performance and instead complicates the model.

However, our study still has several limitations that should be noted. As a retrospective analysis, the predictive models we have developed should undergo further validation in a prospective setting to confirm their efficacy. Besides, our study adopts a single-center design with a limited sample size. Future studies should aim to expand the sample size and include multicenter validations to bolster the generalizability and external validity of the results. Finally, our radiomics analysis is currently confined to specific MRI sequences (FLAIR, T1-CE and ADC), as well as metabolic PET images (^{18}F-FET PET). It is plausible that incorporating dynamic FET PET parameters (e.g., time-activity curves) or advanced MRI sequences, such as dynamic susceptibility contrast perfusion-weighted imaging (DSC-PWI) and diffusion tensor imaging (DTI), might enhance predictive performance by better capturing spatiotemporal heterogeneity.

In conclusion, we developed multiparametric prediction models with simultaneous structural, proliferative, and metabolic information based on ^{18}F-FET PET/MRI radiomics, which can offer significant additional value for the noninvasive preoperative diagnosis of IDH, TERT, and MGMT status in adult diffuse gliomas.

Abbreviations

ADC	Apparent diffusion coefficient
AUC	Area under the receiver operating characteristic curve
DCA	Decision curve analysis
DWI	Diffusion-Weighted Imaging
FLAIR	Fluid-attenuated inversion recovery
^{18}F-FET	O-2-[^{18}F] fluoroethyl-L-tyrosine
IDH	Isocitrate dehydrogenase
MGMT	O6-methylguanine-DNA methyltransferase
MRI	Magnetic resonance imaging
PET	Positron emission tomography
Rad-Score	Radiomics score
ROC	Receiver operating characteristic
TERT	Telomerase reverse transcriptase
T1-CE	Contrast-enhanced T1-weighted magnetic resonance imaging

Supplementary Information

The online version contains supplementary material available at https://doi.org/10.1186/s12880-025-01729-7.

Supplementary Material 1

Acknowledgements

We appreciate Yanmei Wang's assistance in reviewing the statistical aspects of our analysis.

Author contributions

JB and JL contributed to the conception and design of the manuscript. JB, BC, FL, and XH performed data acquisition and drafted the manuscript. BC and HY provided study materials and patient resources. JB conducted the statistical analysis. JL supervised the manuscript and managed the funding acquisition. All authors read and approved the final manuscript.

Funding
This research was supported by the National Key Research and Development Program of China [No. 2022YFC2406900], and the Huizhi Ascent Project of Xuanwu Hospital [HZ2021ZCLJ005].

Data availability
No datasets were generated or analysed during the current study.

Declarations

Ethics approval and consent to participate
In accordance with the Declaration of Helsinki, this retrospective study was approved by the Ethics Committee and Institutional Review Board of Xuanwu Hospital, Capital Medical University (No. 2023-044). Written informed consent was obtained from patients prior to PET/MR scans.

Consent for publication
Informed consent was obtained from the individual and her family, who had signed the power of attorney document.

Competing interests
The authors declare no competing interests.

Received: 25 February 2025 / Accepted: 13 May 2025
Published online: 26 May 2025

References

1. Wen PY, Weller M, Lee EQ, Alexander BM, Barnholtz-Sloan JS, Barthel FP, Batchelor TT, Bindra RS, Chang SM, Chiocca EA, et al. Glioblastoma in adults: a society for Neuro-Oncology (SNO) and European society of Neuro-Oncology (EANO) consensus review on current management and future directions. Neurooncology. 2020;22(8):1073–113.
2. Horbinski C, Nabors LB, Portnow J, Baehring J, Bhatia A, Bloch O, Brem S, Butowski N, Cannon DM, Chao S, et al. NCCN Guidelines® insights: central nervous system cancers, version 2.2022. J Natl Compr Cancer Netw JNCCN. 2023;21(1):12–20.
3. Horbinski C, Berger T, Packer RJ, Wen PY. Clinical implications of the 2021 edition of the WHO classification of central nervous system tumours. Nat Reviews Neurol. 2022;18(9):515–29.
4. Di Nunno V, Franceschi E, Tosoni A, Gatto L, Maggio I, Lodi R, Angelini D, Bartolini S, Brandes AA. Clinical and molecular features of patients with gliomas harboring IDH1 Non-canonical mutations: A systematic review and Meta-Analysis. Adv Therapy. 2022;39(1):165–77.
5. Park JW. Metabolic rewiring in Adult-Type diffuse gliomas. Int J Mol Sci. 2023;24(8):7348.
6. Vallée A, Lecarpentier Y, Vallée JN. Opposed interplay between IDH1 mutations and the WNT/β-Catenin pathway: added information for glioma classification. Biomedicines. 2021;9(6):619.
7. Ohba S, Kuwahara K, Yamada S, Abe M, Hirose Y. Correlation between IDH, ATRX, and TERT promoter mutations in glioma. Brain Tumor Pathol. 2020;37(2):33–40.
8. Powter B, Jeffreys SA, Sareen H, Cooper A, Brungs D, Po J, Roberts T, Koh ES, Scott KF, Sajinovic M, et al. Human TERT promoter mutations as a prognostic biomarker in glioma. J Cancer Res Clin Oncol. 2021;147(4):1007–17.
9. Labussière M, Boisselier B, Mokhtari K, Di Stefano AL, Rahimian A, Rossetto M, Ciccarino P, Saulnier O, Paterra R, Marie Y, et al. Combined analysis of TERT, EGFR, and IDH status defines distinct prognostic glioblastoma classes. Neurology. 2014;83(13):1200–6.
10. Richardson TE, Walker JM, Hambardzumyan D, Brem S, Hatanpaa KJ, Viapiano MS, Pai B, Umphlett M, Becher OJ, Snuderl M, et al. Genetic and epigenetic instability as an underlying driver of progression and aggressive behavior in IDH-mutant Astrocytoma. Acta Neuropathol. 2024;148(1):5.
11. Zhao B, Wu J, Xia Y, Li H, Wang Y, Qu T, Xing H, Wang Y, Ma W. Comparative efficacy and safety of therapeutics for elderly glioblastoma patients: A bayesian network analysis. Pharmacol Res. 2022;182:106316.
12. Arita H, Yamasaki K, Matsushita Y, Nakamura T, Shimokawa A, Takami H, Tanaka S, Mukasa A, Shirahata M, Shimizu S, et al. A combination of TERT promoter mutation and MGMT methylation status predicts clinically relevant subgroups of newly diagnosed glioblastomas. Acta Neuropathol Commun. 2016;4(1):79.
13. Song S, Cheng Y, Ma J, Wang L, Dong C, Wei Y, Xu G, An Y, Qi Z, Lin Q, et al. Simultaneous FET-PET and contrast-enhanced MRI based on hybrid PET/MR improves delineation of tumor Spatial biodistribution in gliomas: a biopsy validation study. Eur J Nucl Med Mol Imaging. 2020;47(6):1458–67.
14. Song S, Wang L, Yang H, Shan Y, Cheng Y, Xu L, Dong C, Zhao G, Lu J. Static ^{18}F-FET PET and DSC-PWI based on hybrid PET/MR for the prediction of gliomas defined by IDH and 1p/19q status. Eur Radiol. 2021;31(6):4087–96.
15. Maurer GD, Brucker DP, Stoffels G, Filipski K, Filss CP, Mottaghy FM, Galldiks N, Steinbach JP, Hattingen E, Langen KJ. ^{18}F-FET PET imaging in differentiating glioma progression from Treatment-Related changes: A Single-Center experience. Journal of nuclear medicine: official publication. Soc Nuclear Med. 2020;61(4):505–11.
16. Albert NL, Galldiks N, Ellingson BM, van den Bent MJ, Chang SM, Cicone F, de Groot J, Koh ES, Law I, Le Rhun E, et al. PET-based response assessment criteria for diffuse gliomas (PET RANO 1.0): a report of the RANO group. Lancet Oncol. 2024;25(1):e29–41.
17. Liesche F, Lukas M, Preibisch C, Shi K, Schlegel J, Meyer B, Schwaiger M, Zimmer C, Förster S, Gempt J, et al. ^{18}F-Fluoroethyl-tyrosine uptake is correlated with amino acid transport and neovascularization in treatment-naive glioblastomas. Eur J Nucl Med Mol Imaging. 2019;46(10):2163–8.
18. Ren S, Tang HJ, Zhao R, Duan SF, Chen R, Wang ZQ. Application of unenhanced computed tomography texture analysis to differentiate pancreatic adenosquamous carcinoma from pancreatic ductal adenocarcinoma. Curr Med Sci. 2022;42(1):217–25.
19. Zaragori T, Oster J, Roch V, Hossu G, Chawki MB, Grignon R, Pouget C, Gauchotte G, Rech F, Blonski M, et al. ^{18}F -FDOPA PET for the noninvasive prediction of glioma molecular parameters: A radiomics study. Journal of nuclear medicine: official publication. Soc Nuclear Med. 2022;63(1):147–57.
20. Zhou W, Huang Q, Wen J, Li M, Zhu Y, Liu Y, Dai Y, Guan Y, Zhou Z, Hua T. Integrated CT radiomics features could enhance the efficacy of ^{18}F-FET PET for Non-Invasive isocitrate dehydrogenase genotype prediction in adult untreated gliomas: A retrospective cohort study. Front Oncol. 2021;11:772703.
21. Kaiser L, Quach S, Zounek AJ, Wiestler B, Zatcepin A, Holzgreve A, Bollenbacher A, Bartos LM, Ruf VC, Böning G, et al. Enhancing predictability of IDH mutation status in glioma patients at initial diagnosis: a comparative analysis of radiomics from MRI, [^{18}F]FET PET, and TSPO PET. Eur J Nucl Med Mol Imaging. 2024;51(8):2371–81.
22. Bauer EK, Stoffels G, Blau T, Reifenberger G, Felsberg J, Werner JM, Lohmann P, Rosen J, Ceccon G, Tscherpel C, et al. Prediction of survival in patients with IDH-wildtype astrocytic gliomas using dynamic O-(2-[^{18}F]-fluoroethyl)-L-tyrosine PET. Eur J Nucl Med Mol Imaging. 2020;47(6):1486–95.
23. Li X, Cheng Y, Han X, Cui B, Li J, Yang H, Xu G, Lin Q, Xiao X, Tang J, et al. Exploring the association of glioma tumor residuals from incongruent [^{18}F] FET PET/MR imaging with tumor proliferation using a multiparametric MRI radiomics nomogram. Eur J Nucl Med Mol Imaging. 2024;51(3):779–96.
24. Berger TR, Wen PY, Lang-Orsini M, Chukwueke UN. World health organization 2021 classification of central nervous system tumors and implications for therapy for Adult-Type gliomas: A review. JAMA Oncol. 2022;8(10):1493–501.
25. Eckel-Passow JE, Lachance DH, Molinaro AM, Walsh KM, Decker PA, Sicotte H, Pekmezci M, Rice T, Kosel ML, Smirnov IV, et al. Glioma groups based on 1p/19q, IDH, and TERT promoter mutations in tumors. N Engl J Med. 2015;372(26):2499–508.
26. Whitfield BT. JT Huse.Classification of adult-type diffuse gliomas: Impact of the World Health Organization 2021 update. Brain Pathol. (Zurich, Switzerland). 2022;32(4):e13062.
27. Lohmeier J, Radbruch H, Brenner W, Hamm B, Tietze A, Makowski MR. Predictive IDH Genotyping Based on the Evaluation of Spatial Metabolic Heterogeneity by Compartmental Uptake characteristics in Preoperative Glioma Using ^{18}F-FET PET. Journal of nuclear medicine: official publication. Soc Nuclear Med. 2023;64(11):1683–9.
28. Bashir A, Mathilde Jacobsen S, Mølby Henriksen O, Broholm H, Urup T, Grunnet K, Andrée Larsen V, Møller S, Skjøth-Rasmussen J, Skovgaard Poulsen H, et al. Recurrent glioblastoma versus late posttreatment changes: diagnostic accuracy of O-(2-[^{18}F]fluoroethyl)-L-tyrosine positron emission tomography (^{18}F-FET PET). Neurooncology. 2019;21(12):1595–606.
29. Verger A, Stoffels G, Bauer EK, Lohmann P, Blau T, Fink GR, Neumaier B, Shah NJ, Langen KJ, Galldiks N. Static and dynamic ^{18}F-FET PET for the characterization of gliomas defined by IDH and 1p/19q status. Eur J Nucl Med Mol Imaging. 2018;45(3):443–51.

30. Vettermann F, Suchorska B, Unterrainer M, Nelwan D, Forbrig R, Ruf V, Wenter V, Kreth FW, Herms J, Bartenstein P, et al. Non-invasive prediction of IDH-wildtype genotype in gliomas using dynamic ^{18}F-FET PET. Eur J Nucl Med Mol Imaging. 2019;46(12):2581–25898.
31. Song S, Shan Y, Wang L, Cheng Y, Yang H, Zhao G, Wang Z, Lu J. MGMT promoter methylation status shows no effect on [^{18}F]FET uptake and CBF in gliomas: a stereotactic image-based histological validation study. Eur Radiol. 2022;32(8):5577–87.
32. Unterrainer M, Ruf V, von Rohr K, Suchorska B, Mittlmeier LM, Beyer L, Brendel M, Wenter V, Kunz WG, Bartenstein P, et al. TERT-Promoter mutational status in Glioblastoma - Is there an association with amino acid uptake on dynamic ^{18}F-FET PET? Frontiers in oncology. 2021;11:645316.
33. Li Z, Holzgreve A, Unterrainer LM, Ruf VC, Quach S, Bartos LM, Suchorska B, Niyazi M, Wenter V, Herms J, et al. Combination of pre-treatment dynamic [^{18}F]FET PET radiomics and conventional clinical parameters for the survival stratification in patients with IDH-wildtype glioblastoma. Eur J Nucl Med Mol Imaging. 2023;50(2):535–45.
34. Li Z, Kaiser L, Holzgreve A, Ruf VC, Suchorska B, Wenter V, Quach S, Herms J, Bartenstein P, Tonn JC, et al. Prediction of TERTp-mutation status in IDH-wildtype high-grade gliomas using pre-treatment dynamic [^{18}F]FET PET radiomics. Eur J Nucl Med Mol Imaging. 2021;48(13):4415–25.
35. Kim M, Jung SY, Park JE, Jo Y, Park SY, Nam SJ, Kim JH, Kim HS. Diffusion- and perfusion-weighted MRI radiomics model May predict isocitrate dehydrogenase (IDH) mutation and tumor aggressiveness in diffuse lower grade glioma. Eur Radiol. 2020;30(4):2142–51.
36. Yan J, Zhang B, Zhang S, Cheng J, Liu X, Wang W, Dong Y, Zhang L, Mo X, Chen Q, et al. Quantitative MRI-based radiomics for noninvasively predicting molecular subtypes and survival in glioma patients. NPJ Precision Oncol. 2021;5(1):72.

Publisher's note